*Integrated Systems and Technologies*

Cancer Research

# Noninvasive Detection of Target Modulation following Phosphatidylinositol 3-Kinase Inhibition Using Hyperpolarized $^{13}C$ Magnetic Resonance Spectroscopy

Christopher S. Ward[1], Humsa S. Venkatesh[1], Myriam M. Chaumeil[1], Alissa H. Brandes[1], Mark VanCriekinge[1], Hagit Dafni[1], Subramaniam Sukumar[1], Sarah J. Nelson[1], Daniel B. Vigneron[1], John Kurhanewicz[1], C. David James[2], Daphne A. Haas-Kogan[2], and Sabrina M. Ronen[1]

## Abstract

Numerous mechanism-based anticancer drugs that target the phosphatidylinositol 3-kinase (PI3K) pathway are in clinical trials. However, it remains challenging to assess responses by traditional imaging methods. Here, we show for the first time the efficacy of hyperpolarized $^{13}C$ magnetic resonance spectroscopy (MRS) in detecting the effect of PI3K inhibition by monitoring hyperpolarized [1-$^{13}C$]lactate levels produced from hyperpolarized [1-$^{13}C$]pyruvate through lactate dehydrogenase (LDH) activity. In GS-2 glioblastoma cells, PI3K inhibition by LY294002 or everolimus caused hyperpolarized lactate to drop to 42 ± 12% and to 76 ± 5%, respectively. In MDA-MB-231 breast cancer cells, hyperpolarized lactate dropped to 71 ± 15% after treatment with LY294002. These reductions were correlated with reductions in LDH activity to 48 ± 4%, 63 ± 4%, and 69 ± 12%, respectively, and were associated with a drop in levels of LDHA mRNA and LDHA and hypoxia-inducible factor-1α proteins. Supporting these findings, tumor growth inhibition achieved by everolimus in murine GS-2 xenografts was associated with a drop in the hyperpolarized lactate-to-pyruvate ratio detected by *in vivo* MRS imaging, whereas an increase in this ratio occurred with tumor growth in control animals. Taken together, our findings illustrate the application of hyperpolarized $^{13}C$ MRS of pyruvate to monitor alterations in LDHA activity and expression caused by PI3K pathway inhibition, showing the potential of this method for noninvasive imaging of drug target modulation. *Cancer Res; 70(4); 1296–305. ©2010 AACR.*

## Introduction

The phosphatidylinositol 3-kinase (PI3K) pathway plays an integral role in the regulation of many key cellular processes, mediating proliferation, differentiation, intracellular signaling, and glucose metabolism (1). Constitutive signaling through deregulation of the pathway is common in human cancers and drives tumor development by inducing angiogenesis, motility, invasion, progression, and survival (2). The PI3K pathway is one of the most frequently activated, with current estimates indicating that mutations in at least one of the pathway components account for up to 30% of all sporadic human cancers (3, 4). Given the importance of this signaling pathway in oncogenesis, it provides an attractive target for mechanism-based anticancer treatments (5, 6). Accordingly, several PI3K inhibitors are currently in clinical trials with promising results in glioblastoma, breast, hematologic, and non–small cell lung cancer studies (7).

Response to PI3K inhibition is often associated with tumor stasis rather than shrinkage (8, 9). Consequently, the utility of such traditional imaging methods as computed tomography and magnetic resonance imaging (MRI) in monitoring early response is limited. Current clinical trials resort to either indirect methods, such as inspection of peripheral blood mononuclear cells for drug-induced molecular effects, or highly invasive methods, such as monitoring of sequential tumor biopsies (10, 11). For this reason, identifying novel biomarkers of target inhibition that are detectable by noninvasive methods is essential for determining the efficacy of treatment and correlation with antitumor effects (7, 12).

Magnetic resonance spectroscopy (MRS) is a noninvasive, radiation-free method that has been valuable for informing on biochemical composition of cancer cells and providing metabolic imaging biomarkers of cell transformation and response to treatment (13–18). We have used MRS to identify biomarkers of response to emerging targeted therapies (19–23). In particular, we have shown that inhibition of the PI3K pathway by LY294002 or wortmannin is associated in cells with a drop in phosphocholine (PC; ref. 22). Consistent with this finding, *in vivo* treatment with the bioavailable wortmannin analogue PX-866 resulted in a drop in choline-containing metabolites in an orthotopic brain tumor model (23).

**Authors' Affiliations:** Departments of [1]Radiology and Biomedical Imaging and [2]Neurological Surgery, University of California at San Francisco, San Francisco, California

**Note:** C.S. Ward and H.S. Venkatesh contributed equally to this work.

**Corresponding Author:** Sabrina M. Ronen, Department of Radiology and Biomedical Imaging, University of California at San Francisco, 1700 4th Street, San Francisco, CA 94158. Phone: 415-514-4839; Fax: 415-514-2550; E-mail: sabrina.ronen@radiology.ucsf.edu.

**doi:** 10.1158/0008-5472.CAN-09-2251

$^{13}$C MRS methods can also be used to inform on cellular metabolism, but application has been limited due to low sensitivity. However, recent advances in dynamic nuclear polarization (DNP) and its application to solution-state MR provide a signal enhancement of >10,000-fold compared with conventional $^{13}$C MRS (24). The dramatically improved signal-to-noise ratio has enabled the real-time investigation of previously unexplored metabolic reactions (25–29). In particular, this method has been used to monitor pyruvate metabolism *in vivo* and in cells to show an increase in pyruvate-to-lactate conversion in cancer, consistent with the increase in LDH activity (25, 29). In a prostate cancer model, elevated hyperpolarized lactate and an increase in the ratio of hyperpolarized lactate to total hyperpolarized carbon species were associated with histologic grade (29). In other studies, a drop in hyperpolarized lactate formation was observed following chemotherapeutic treatment, a result of the apoptotically induced depletion of NADH, the cofactor of LDH (27).

Hyperpolarized $^{13}$C MRS of pyruvate has unrealized potential for monitoring therapies specifically targeted at key carcinogenic pathways. The modulation of energy production and its interplay with altered cell signaling has received substantial attention in recent years (30, 31) and it is clear that PI3K signaling has direct effects on glucose metabolism (32). Several putative interactions exist but it is likely that the predominant link is through mammalian target of rapamycin (mTOR)–activated posttranscriptional control of hypoxia-inducible factor-1 (HIF-1; refs. 33–35), which controls the expression of several glycolytic enzymes, including the LDH subunit LDHA (32, 36, 37). Based on this knowledge, we hypothesized that PI3K signaling would directly affect cellular LDH activity and that this could be monitored using hyperpolarized $^{13}$C MRS by observing the formation of hyperpolarized lactate from introduced hyperpolarized pyruvate. Treatment with a PI3K inhibitor would negatively modulate hyperpolarized lactate formation. Hyperpolarized lactate would thus provide a biomarker of PI3K signaling inhibition.

To test this hypothesis, we investigated two cancer cell lines treated with inhibitors of PI3K signaling. We observed that signal inhibition resulted in a significant reduction in hyperpolarized lactate and show that this reduction is due to partial silencing of HIF-1–regulated expression of LDHA and a resulting drop in LDH activity. Our results indicate, to our knowledge for the first time, that hyperpolarized $^{13}$C MRS could be used to monitor PI3K signal inhibition and thus can address the need for a noninvasive approach to monitor the efficacy of PI3K-targeted drug treatments.

## Materials and Methods

***Cell culture.*** GS-2 cells were supplied by Dr. Haas-Kogan and Dr. James (University of California, San Francisco, CA) and MDA-MB-231 cells by Dr. Lotan (University of Texas M.D. Anderson Cancer Center, Houston, TX). Unique DNA "fingerprint" identities (i.e., variable number tandem repeat PCR products) have been established for the cell lines used in this study, and the identities of these cell lines were confirmed in association with their use in the experiments described here.

Cells were cultured in DMEM supplemented with 10% heat-inactivated fetal bovine serum, 2 mmol/L L-glutamine, 100 units/mL penicillin, and 100 μg/mL streptomycin. DMEM used for culturing of GS-2 was supplemented with an additional 1 mmol/L sodium pyruvate and 28 mmol/L glucose. Custom-made DMEM with 0.22 g/L inorganic phosphate [$P_i$; University of California at San Francisco (UCSF) Cell Culture Facility] was used in MRS studies. For all experiments, cells were harvested in their logarithmic phase of proliferation.

For PI3K inhibition, cells were incubated with 50 μmol/L LY294002. GS-2 cells were treated for 48 h and MDA-MB-231 cells were treated for 40 h, based on previous work (22). For mTOR inhibition, cells were treated for 48 h with 100 nmol/L everolimus (Molcan Corp.). To monitor the effect of a DNA-damaging agent, cells were treated for 48 h with 100 μmol/L temozolomide (Tecoland Corp.). The final concentration of DMSO used to dissolve all inhibitors was 1:1,000 in culture medium.

***Cell proliferation assay.*** The effect of drug treatment on cell proliferation was determined using the WST-1 reagent assay (Roche). Cells were seeded in 96-well plates and treated for 4 to 48 h. After treatment, WST-1 reagent was incubated in wells for 2 h and cell viability was determined by quantification of absorbance at 440 nm using a spectrophotometer (Tecan).

***Perfused cell system setup.*** For MRS studies, cells were encapsulated in agarose beads, essentially as described (38). The same number of cells ($1.5 \times 10^8$ to $2 \times 10^8$ for GS-2 and $7 \times 10^7$ to $8 \times 10^7$ for MDA-MB-231) was investigated in both control and treated experiments. After encapsulation, beads were incubated overnight in growth medium before MRS experiments.

The beads were loaded into a nuclear magnetic resonance (NMR)–compatible perfusion system, modified as previously described (38). Briefly, the perfusion system consisted of three tubing lines to circulate medium to a 10-mm NMR tube and one tubing line to deliver 5% $CO_2$. A three-way valve allowed for introduction of hyperpolarized material to the inflow line. Perfusion medium (100 mL) was circulated at 1.5 mL/min throughout the MRS studies. Medium circulation was stopped briefly during injection of hyperpolarized pyruvate and acquisition of $^{13}$C spectra. The NMR probe was maintained at 35°C.

***$^{31}$P MRS acquisition and analysis.*** $^{31}$P MRS spectra were acquired on a 500-MHz INOVA spectrometer (Varian) using a pulse-acquire scheme [30° pulse, 3-s repetition time (TR)] and composite pulse $^1$H decoupling during acquisition. The resulting spectra were analyzed using ACD/Spec Manager version 9.15 (Advanced Chemistry Development). Metabolite concentrations were calculated from peak areas determined by deconvolution, with correction for saturation and normalization to both internal reference ($P_i$, 1.87 μmol/L) and cell number.

***Hyperpolarization.*** Samples of [1-$^{13}$C]pyruvic acid (Isotech) containing 15 mmol/L of the trityl radical OX063 (Oxford Instruments) were hyperpolarized using the Hypersense DNP (Oxford Instruments) polarizer as described (26, 29). After 1.5 h, polarized pyruvic acid was rapidly dissolved in

6.0 mL of isotonic 40 mmol/L Tris-based buffer containing 3.0 μmol/L EDTA (pH 7.8) and injected into the perfusion system within 15 s.

***$^{13}$C MRS acquisition and analysis.*** Single-transient $^{13}$C spectra were acquired every 3 s for 300 s. In experiments with GS-2 cells, 13° excitation pulses were used. Experiments with MDA-MB-231 used 5° pulses. The intensities of lactate peaks were quantified by integration using ACD/Spec Manager. To correct for small variations in the degree of polarization, peak area values of individual hyperpolarized species were normalized to the peak area of all hyperpolarized species at maximum value (predominantly pyruvate, occurring immediately after injection). In addition, values were normalized to cell number.

Two approaches were used to determine the effect of PI3K inhibition on hyperpolarized lactate formation. First, maximum lactate levels per cell ($Lac_{max}$) were determined and compared in control and treated cells exposed to the same pyruvate concentrations. Second, the apparent pseudorate of lactate production was determined and compared. For this, we used Bloch equations modified for two-site chemical exchange similarly to previously described (39). Briefly, we considered the chemical equilibrium between pyruvate (Pyr) and lactate (Lac) catalyzed by LDH (Eq. A):

$$Pyruvate \underset{k_{Lac}}{\overset{k_{Pyr}}{\rightleftarrows}} Lactate \qquad (A)$$

where $k_{Pyr}$ and $k_{Lac}$ are the unidirectional rate constants of pyruvate-to-lactate conversion and lactate-to-pyruvate conversion, respectively. After injection of hyperpolarized [1-$^{13}$C]pyruvate, the time courses of pyruvate and lactate longitudinal magnetizations, $Pyr_z(t)$ and $Lac_z(t)$, were modeled (Eqs. B and C):

$$\frac{dPyr_z(t)}{dt} = -\rho_{Pyr}(Pyr_z(t) - Pyr_{z\infty}) - k_{Pyr}Pyr_z(t) + k_{Lac}Lac_z(t) \qquad (B)$$

$$\frac{dLac_z(t)}{dt} = -\rho_{Lac}(Lac_z(t) - Lac_{z\infty}) + k_{Pyr}Pyr_z(t) - k_{Lac}Lac_z(t) \qquad (C)$$

where $\rho_{Pyr}$ and $\rho_{Lac}$ are the spin lattice relaxation rates [$1/T_{1\,(Pyr,\ Lac)}$], $t$ is time, and $Pyr_{z\infty}$ and $Lac_{z\infty}$ are the equilibrium magnetizations of Pyr and Lac, respectively. Using these equations, the peak integrals of pyruvate and lactate versus time were fit using a nonlinear least-squares algorithm implemented in Matlab (The MathWorks, Inc.), leading to the estimation of $k_{Pyr}$, $k_{Lac}$, and $\rho_{Pyr} = \rho_{Lac}$. Monte Carlo simulation was also performed to assess the accuracy on the three fitted parameters.

***LDH activity.*** The activity of LDH was measured in cell lysates by monitoring NADH consumption after addition of varying concentrations of pyruvate as described (40) by monitoring absorbance at 340 nm for 10 min using an Infinite M200 spectrophotometer (Tecan). $K_M$ and $V_{max}$ values were then determined by fitting the initial velocity plots using a Lineweaver-Burke plot.

***Gene expression of LDHA.*** Total cellular RNA was extracted by RNeasy Mini kit (Qiagen). The quantity of total RNA was determined using a NanoDrop ND1000 Fluorospectrometer (NanoDrop Technologies). Reverse transcription was performed using the QuantiTect Reverse Transcription kit (Qiagen). Real-time PCR of resulting cDNA was performed on a Taqman 7900 (Applied Biosystems). Expression of LDHA was examined using Assays-on-Demand (Applied Biosystems) and compared with the housekeeping gene *β-actin* (Integrated DNA Technologies). All procedures were performed according to the manufacturers' instructions.

***PI3K pathway protein levels.*** The effect of PI3K signaling inhibition on PI3K pathway protein levels was analyzed by Western blotting. Cytoplasmic and nuclear proteins were run on 4% to 20% gels (Bio-Rad) by SDS-PAGE method; electrotransferred onto nitrocellulose membranes; blocked and incubated with primary antibodies anti–4E-BP1, anti–phosphorylated 4E-BP1 (p-4E-BP1; Ser$^{65}$), anti–glyceraldehyde-3-phosphate dehydrogenase (GAPDH), anti–HIF-1α, anti-LDHA (Cell Signaling), and anti-LDHB (Epitomics), and then incubated with secondary antibody anti-IgG horseradish peroxidase–linked antibody (Cell Signaling). Immunocomplexes were visualized using ECL Western Blotting Substrate (Pierce).

***NAD$^+$/NADH assay.*** Concentrations of NAD$^+$ and NADH were measured in cell extracts using an enzyme cycling method and monitoring absorbance at 570 nm as described (41).

***Animals studies.*** All experimental procedures were approved by the UCSF Institutional Animal Care and Use Committee. For tumor implantation, 4-wk-old athymic mice (*nu/nu* homozygous) were anesthetized using a mixture of ketamine/xylazine (100/20 mg/kg), and GS-2 cells (~$1 \times 10^7$) were injected s.c. in the flank. Tumor growth was monitored weekly by caliper measurement until tumors reached ~6 mm in diameter. From that point, treated animals received a daily injection of everolimus (10 mg/kg/d i.p. in 20 μL), whereas control animals were injected daily with carrier (DMSO).

*In vivo* MR studies were performed on a 600-MHz wide bore vertical system (Varian). MRI was performed using a Varian millipede $^1$H coil. A 20-mm home-built $^{13}$C surface coil, positioned at the center of the magnet and of the imaging coil, was used for hyperpolarized MRS studies. Mice were anesthetized using isoflurane (3% in $O_2$, 1.5 L/min), and a catheter was secured in the tail vein. Following initial knockdown of animals, anesthesia was maintained at 0.5-1.5% in $O_2$; 1.5 L/min throughout the imaging experiment. The tumor region was placed in the center of the $^{13}$C coil, and the animal was positioned in the center of the magnet using a custom-built cradle. A glass tube containing $^{13}$C-enriched urea placed at the center of the surface coil was used for position and chemical shift reference.

Anatomic imaging was performed first to assess the positioning and size of the tumor [two-dimensional spin echo (SE); echo time (TE)/TR = 20/2,000 ms; field of view (FOV) = 32 × 32 mm; matrix 256 × 256; slice thickness = 0.5 mm; gap = 0.5 mm; Tacq = 8 min and 32 s; number of transients (NT) = 2]. [1-$^{13}$C]Pyruvic acid was hyperpolarized as above. Three hundred microliters of 100 mmol/L hyperpolarized pyruvic acid in

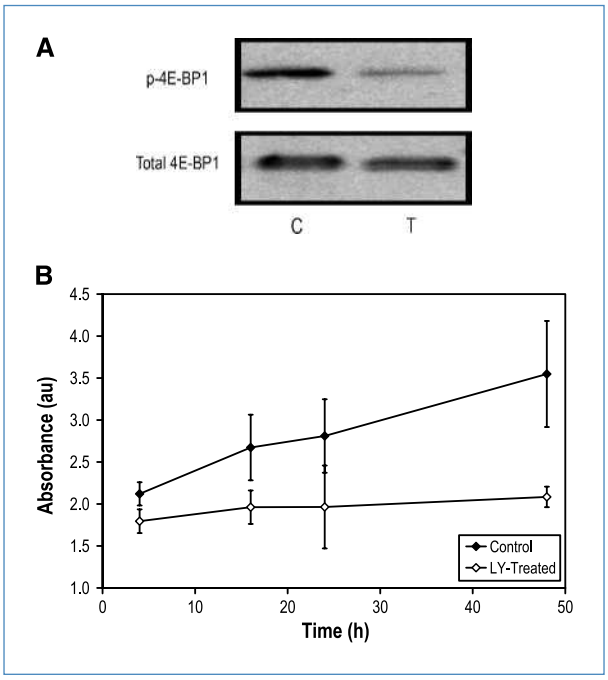


Figure 1. Effect of LY294002 on PI3K signaling in GS-2 cells. A, Western blots showing depletion of p-4E-BP1 levels in GS-2 following a 48-h exposure to 50 μmol/L LY294002. Total 4E-BP1 is shown as a loading control. B, WST-1 cell proliferation assay showing a reduction in the proliferation rate over 48 h.

40 mmol/L Tris, 100 mmol/L NaOH, and 0.1 mg/L $Na_2EDTA$ were then injected via the catheter over 12 s, and $^{13}$C two-dimensional MRS imaging (MRSI) was acquired 37 s after injection, the time point when, based on nonlocalized $^{13}$C dynamic data, the hyperpolarized $^{13}$C lactate reached a maximum as previously described (42). The $^{13}$C two-dimensional magnetic resonance spectroscopic imaging (MRSI) parameters were as follows: TE/TR = 0.195/125 ms; frequency dimension = 512; phase dimension = 8 × 8; spectral width (SW) = 5,000 Hz; FOV = 32 × 32 mm; Tacq = 8 s. A rectangular pulse, equivalent to a 20° flip angle at 5 mm from the coil, was used for excitation.

Tumor volume was calculated from caliper measurements and confirmed from SE images assuming an ellipsoid shape (volume = $4/3.\pi.a.b.c$). $^{13}$C two-dimensional MRSI data were processed using jMRUI software (43). For each voxel, the amplitudes of lactate and pyruvate were quantified using the AMARES package for MRSI and the lactate-to-pyruvate ratio was calculated as the ratio of the amplitudes (42). From the overlap between anatomic images and MRSI data, the voxels representing >75% tumor were considered as tumor voxels and the lactate-to-pyruvate ratios from these voxels were averaged.

***Statistical analysis.*** Two-tailed unpaired Student's *t* test was used to verify the statistical significance of the results, with $P \leq 0.05$ considered to be significant. All results are expressed as mean ± SD and represent an average of three repeats unless otherwise stated.

## Results

In this study, we monitored the effect of PI3K inhibition on cellular metabolism. We first investigated the GS-2 glioblastoma cell line and then assessed the generality of our findings by investigating the MDA-MB-231 breast cancer cell line and by probing GS-2 xenografts.

***LY294002 leads to inhibition of signaling and cell proliferation in GS-2 cells.*** The effectiveness of LY294002 in achieving suppression of signal propagation through the PI3K pathway in treated GS-2 cells was first assessed by probing p-4E-BP1 downstream of mTOR. Western blotting revealed that p-4E-BP1 was substantially lower following LY294002 treatment, confirming signaling blockage (Fig. 1A).

Consistent with inhibition of PI3K signaling, cessation of proliferation was seen after treatment (Fig. 1B). The WST-1 cell proliferation assay showed that, after 48 hours, the number of treated cells had increased only 49 ± 10% ($P$ = 0.01), whereas the number of control cells increased 385 ± 84% ($P$ = 0.03), resulting in a significant difference between control and LY294002-treated samples ($P$ = 0.02).

***Hyperpolarized $^{13}$C MRS detects a drop in hyperpolarized lactate following PI3K inhibition in GS-2 cells.*** Hyperpolarized $^{13}$C MRS dynamic studies were performed using

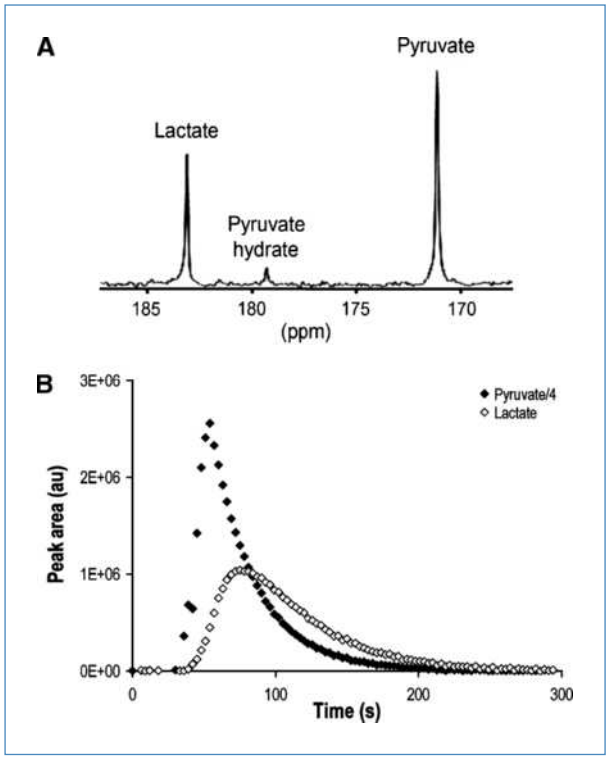


Figure 2. Conversion of hyperpolarized [1-$^{13}$C]pyruvate to [1-$^{13}$C]lactate in a GS-2 perfused cell experiment. A, representative $^{13}$C spectrum 45 s after the addition of hyperpolarized [1-$^{13}$C]pyruvate (final concentration of 1 mmol/L). Resonances for pyruvate, pyruvate hydrate, and lactate are indicated. B, peak areas of hyperpolarized pyruvate (note that the pyruvate peak areas were divided by 4) and lactate during acquisition of 1 mmol/L hyperpolarized pyruvate injection.

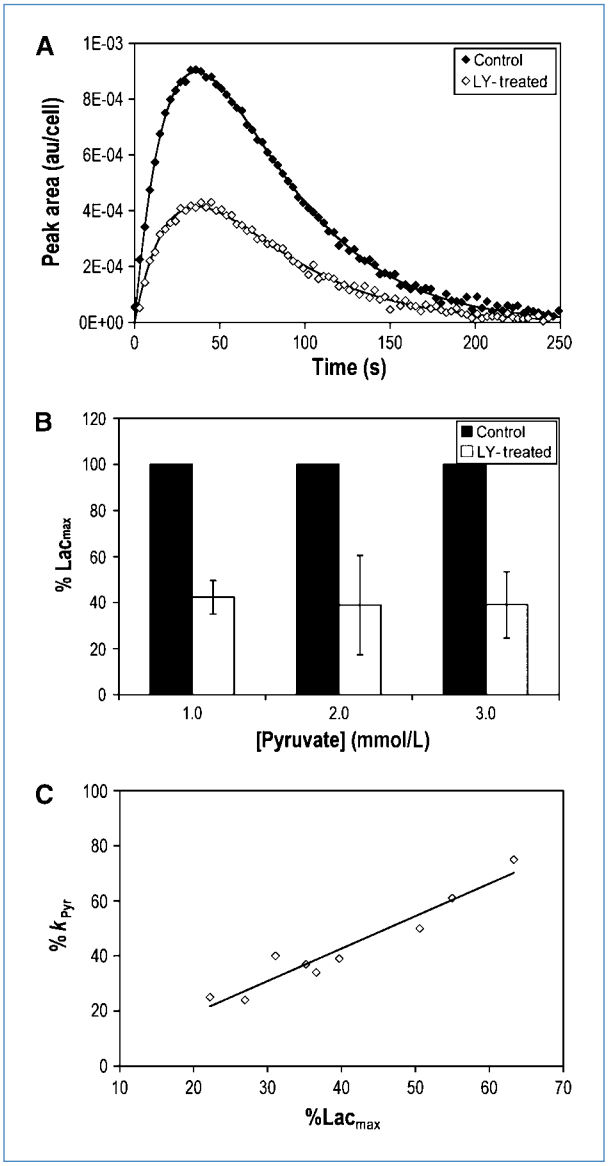


Figure 3. Effect of PI3K inhibition by LY294002 on hyperpolarized lactate formation in GS-2 perfused cells. A, evolution of [1-$^{13}$C]lactate peak areas after addition of 1 mmol/L hyperpolarized [1-$^{13}$C]pyruvate to control or LY294002-treated perfused GS-2 cells, showing reduction in hyperpolarized lactate formation with treatment. Continuous lines represent the fits to Bloch equations. B, reproducible reductions in maximum hyperpolarized lactate ($Lac_{max}$) levels in response to treatment over several concentrations of hyperpolarized pyruvate, indicating that the use of $Lac_{max}$ to probe the effect of PI3K inhibition is reproducible independent of pyruvate concentration. C, plot of $k_{Pyr}$ versus $Lac_{max}$, indicating a correlation between the two methods of hyperpolarized $^{13}$C data analysis. Line, best linear fit ($R^2$ = 0.93).

hyperpolarized [1-$^{13}$C]pyruvate to visualize the LDH-catalyzed conversion of pyruvate to lactate. Figure 2A is a representative $^{13}$C spectrum recorded following injection of hyperpolarized pyruvate. Resonances from pyruvate (171 ppm), pyruvate hydrate (179 ppm), and lactate (183 ppm) were identified. Buildup of pyruvate occurs immediately after its injection (Fig. 2B). Shortly after hyperpolarized pyruvate reaches the cells, lactate appears as pyruvate undergoes reduction, retaining the polarized label. This results in an initial increase in lactate, after which decay of polarization is evident for both pyruvate and lactate.

Injections resulting in a final concentration of 1.0 mmol/L pyruvate were administered to control and LY294002-treated cells. Conversion of hyperpolarized pyruvate to lactate was observed in both samples. However, treatment with LY294002 caused a clear reduction in hyperpolarized lactate levels (Fig. 3A). To quantify this drop, we determined $Lac_{max}$ in each experiment. $Lac_{max}$ levels dropped in treated cells to 42 ± 7% of control ($P$ = 0.005). To further confirm the effect of PI3K inhibition and ascertain that our observations were not dependent on pyruvate concentration, measurements were repeated at higher concentrations of pyruvate (2 and 3 mmol/L). Similar results were observed (Fig. 3B) over all concentrations and average $Lac_{max}$ in treated cells was 42 ± 12% ($P$ < 0.0001, $n$ = 9) of control.

To further confirm our findings, we used a two-site chemical exchange model to fit the hyperpolarized $^{13}$C MRS data (Fig. 3A, continuous line) and determined the apparent pseudorate constant of pyruvate-to-lactate conversion ($k_{Pyr}$). Comparison of $k_{Pyr}$ also showed a significant reduction with LY294002 treatment over all concentrations. Average $k_{Pyr}$ of treated cells was 43 ± 20% ($P$ < 0.0001, $n$ = 9) of control, similar to the reduction in $Lac_{max}$. The reductions in $k_{Pyr}$ correlated with the reductions in $Lac_{max}$ ($R^2$ = 0.93), indicating that both methods of analysis yield similar results (Fig. 3C). Furthermore, $T_1$ values obtained from the fit showed that treatment did not significantly affect the relaxation of hyperpolarized species and therefore did not present a confounding factor in our studies.

***Modulation of metabolites by PI3K inhibitor treatment was detected by $^{31}$P MRS.*** $^{31}$P spectra of control and treated cells were acquired before and following hyperpolarized $^{13}$C MRS to confirm cell viability during the hyperpolarized study and to detect alterations of endogenous metabolites following PI3K inhibition. Nucleotide triphosphate (NTP) levels increased steadily over the course of all studies, indicating sustained cell viability and confirming that exposure of cells to hyperpolarized pyruvate did not affect cell viability or proliferation (data not shown).

$^{31}$P MR spectra (Fig. 4) also indicated that treatment with LY294002 resulted in a significant drop in PC to 34 ± 9% of control ($P$ = 0.006) and phosphoethanolamine (PE) to 49 ± 7% of control ($P$ = 0.006). NTP levels did not change significantly following inhibitor treatment ($P$ = 0.6).

***The drop in hyperpolarized lactate is associated with a drop in HIF-1α levels, LDH expression, and LDH activity in GS-2 cells.*** Because the conversion of pyruvate to lactate in a cellular system could be affected by several independent processes, it was necessary to ascertain that the decrease in hyperpolarized lactate levels was indeed due to a drop in HIF-1α expression downstream of PI3K inhibition, as hypothesized. To this end, we determined LDH activity, LDH expression, and HIF-1α expression.

LDH activity was measured in lysates of control and treated cells over a range of pyruvate concentrations, allowing for

the determination of the kinetic parameters of the LDH-catalyzed reaction (Fig. 5A). Enzyme $V_{max}$ was 20.6 ± 1.0 μmol NADH/min/$10^7$ cells in control cells. Following PI3K inhibition, the activity decreased significantly to 9.8 ± 0.4 μmol NADH/min/$10^7$ cells, or 48 ± 4% of control ($P$ = 0.008). The drop in cellular LDH activity was, within experimental error, the same as the drop in $Lac_{max}$ observed using hyperpolarized $^{13}$C MRS. The $K_M$ values remained unchanged between control and treated cells ($P$ = 0.29). This suggested that the drop in $Lac_{max}$ was due to a drop in cellular LDH activity, which was caused by a decrease in active enzyme concentration.

To confirm the drop in LDH levels, the effect of LY294002 on LDH expression was determined first by Western blotting to assess protein levels and then by reverse transcription-PCR (RT-PCR) to determine mRNA levels. Western blotting revealed a discernable drop in LDHA protein levels (Fig. 5B), whereas no difference in LDHB levels was seen (data not shown). The mRNA expression levels of LDHA also dropped significantly to 49 ± 16% of control ($P$ = 0.0002; Fig. 5C). Finally, we investigated levels of HIF-1α in control and treated cells. Consistent with HIF-1 being responsible for regulation of LDH expression, LY294002 treatment led to decreased levels of HIF-1α (Fig. 5B). Taken together, these data are in line with the proposed mechanism that the drop in $Lac_{max}$ was a result of reduced cellular LDH activity due to lowered HIF-1α levels following PI3K inhibition.

Additionally, it was necessary to study the effects of LY294002 treatment on NADH, the cofactor of LDH necessary for its activity. Previous studies have shown that reduced hyperpolarized pyruvate-to-lactate flux can be caused by depletion of the NAD(H) pool in apoptotic cells (27). However, we found that PI3K inhibition with LY294002 had no significant effect on the concentration of NADH. NADH levels were 0.997 ± 0.137 nmol/$10^7$ cells in control cells and 0.882 ± 0.098 nmol/$10^7$ cells in treated cells ($P$ = 0.31). The ratio of NADH to total NAD(H) was also not significantly changed, at 0.402 ± 0.014 in control compared with 0.335 ± 0.058 in treated cells ($P$ = 0.18).

***Control studies confirm specificity in GS-2 cells.*** To assess the specificity of our findings, GS-2 cells were also treated with the clinically relevant inhibitor everolimus, which targets mTOR downstream of PI3K, and with temozolomide, a DNA-damaging agent that is not implicated in the PI3K signaling pathway. Treatment with everolimus resulted in inhibition of signaling as evidenced by a drop in p-4E-BP1 levels (data not shown) and inhibition in cell proliferation to 45 ± 9% of control ($P$ = 0.001). In $^{13}$C MRS studies, $Lac_{max}$ dropped to 76 ± 5% of control ($P$ = 0.003, $n$ = 4), and LDH activity

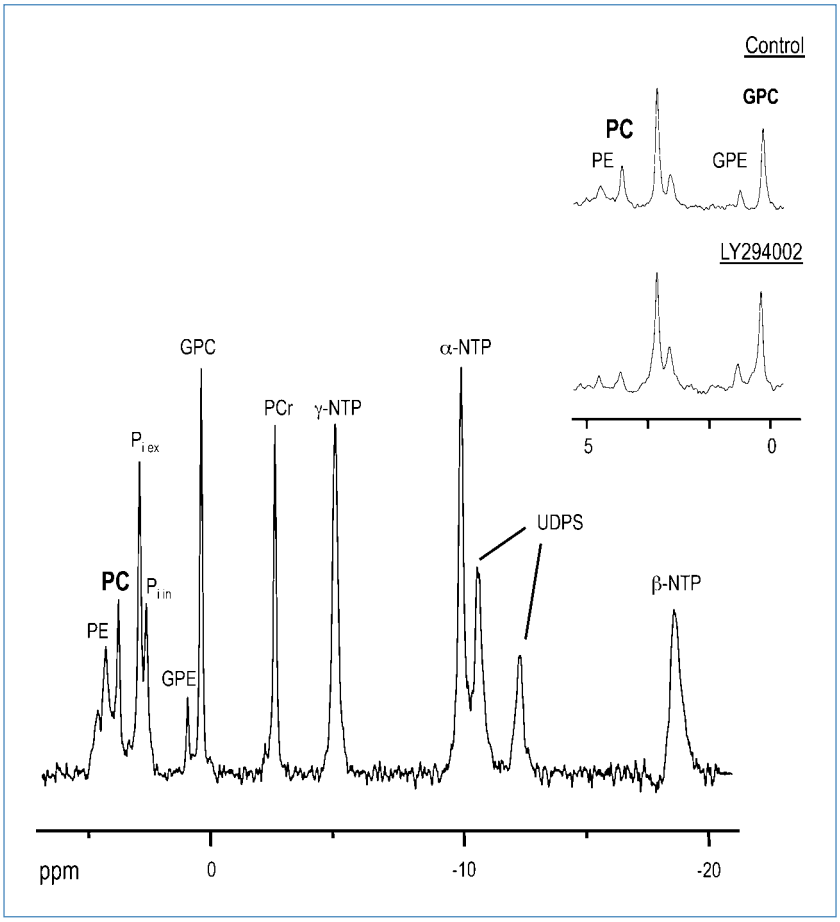


**Figure 4.** Effect of PI3K inhibition on endogenous metabolites detected by $^{31}$P MRS. $^{31}$P MR spectrum obtained from perfused GS-2 cells. Metabolites detectable in spectrum: $P_{i\ ex}$, extracellular $P_i$; $P_{i\ in}$, intracellular $P_i$; GPE, glycerophosphoethanolamine; GPC, glycerophosphocholine; PCr, phosphocreatine; UDPS, UDP-sugars. Inset, expansion of the phosphomonoester and phosphodiester region (0–5 ppm) from control and LY294002-treated cells, indicating a drop in PC and PE in LY294002-treated cells.

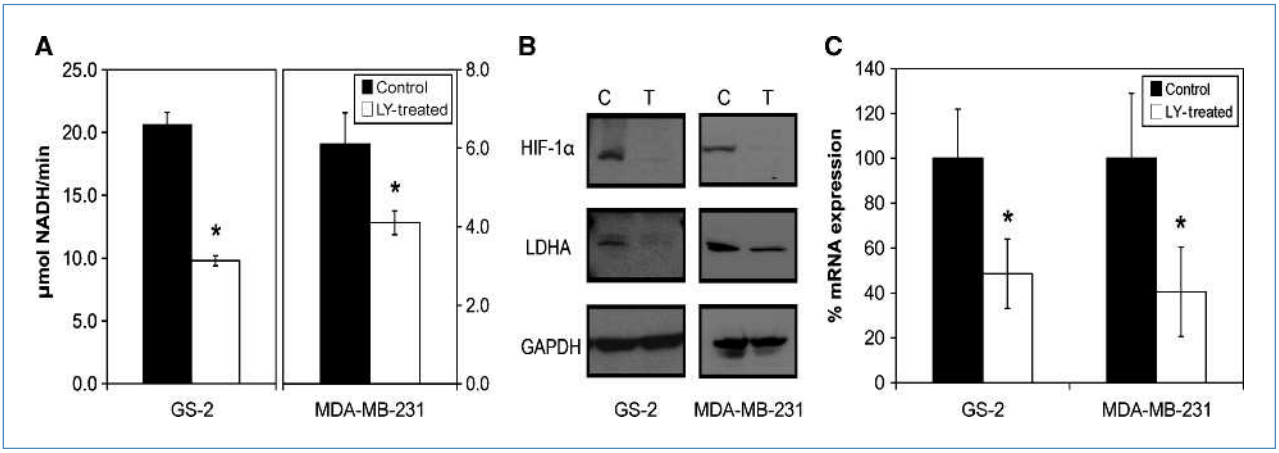


Figure 5. Effect of PI3K inhibition by LY294002 on LDH activity, LDH levels, and HIF-1α levels in GS-2 and MDA-MB-231 cells. A, $V_{max}$ of LDH activity in cell lysates, showing a decrease in the activity with PI3K inhibition. B, Western blot analysis revealing decreases in levels of LDHA and HIF-1α after treatment. GAPDH is shown as a loading control. C, RT-PCR analysis showing a decrease in LDHA gene expression following PI3K inhibition (*, $P < 0.05$).

dropped to 63 ± 4% of control ($P = 0.003$). In contrast, treatment with temozolomide resulted in inhibition in cell proliferation to 70 ± 10% of control ($P = 0.03$), but immunoblotting showed no signal inhibition (data not shown). In line with the unaltered signaling, hyperpolarized $^{13}C$ MRS studies showed no change in $Lac_{max}$ levels ($P > 0.1$, $n = 4$) and LDH activity assays showed no observable differences in $V_{max}$ levels ($P = 0.7$).

***Findings are confirmed in MDA-MB-231 cells.*** To assess the generality of our findings, the effect of PI3K inhibition was also investigated in the human breast adenocarcinoma cell line MDA-MB-231. Similar to GS-2 cells, and as previously reported (22), inhibition of PI3K signaling with LY294002 resulted in decreased cell proliferation and a substantial drop in 4E-BP1 phosphorylation (data not shown).

Hyperpolarized studies were repeated in MDA-MB-231 cells, resulting in similar observations to those made in GS-2 cells. Hyperpolarized lactate levels in treated cells decreased significantly, independent of hyperpolarized pyruvate concentration presented to the cells. On average, $Lac_{max}$ dropped to

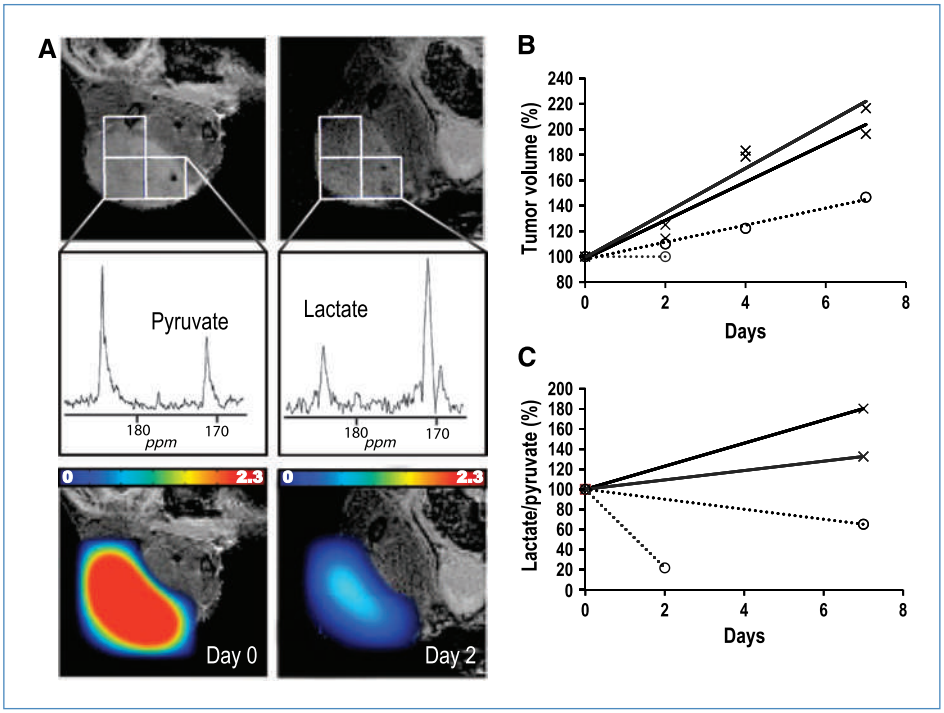


Figure 6. Effect of everolimus treatment on GS-2 tumor xenografts. A, coronal image (7 mm from the surface coil) overlaid with tumor voxels (top) illustrating the origin of two-dimensional averaged MRSI spectra (middle) and overlay of relative lactate-to-pyruvate ratio maps (bottom) before (left) and following 2 d of treatment (right). B, tumor volume in control (continuous lines) and treated (dotted lines) tumors. C, lactate-to-pyruvate ratio in control (continuous lines) and treated (dotted lines) tumors.

71 ± 15% of control ($P = 0.001$, $n = 8$), whereas $k_{Pyr}$ dropped to a comparable 63 ± 38% ($P = 0.02$, $n = 6$).

As illustrated in Fig. 5A, LDH $V_{max}$ decreased significantly to 69 ± 12% in treated cells from 6.1 ± 0.8 μmol NADH/min/$10^7$ cells to 4.1 ± 0.3 μmol NADH/min/$10^7$ cells ($P = 0.01$, $n = 4$). As in GS-2 cells, the drop in LDH activity was, within experimental error, the same as the drop in $Lac_{max}$. $K_M$ remained unchanged ($P = 0.91$, $n = 4$). Western blots revealed a drop in LDHA as well as in HIF-1α in LY294002-treated cells compared with controls (Fig. 5B), whereas there was no apparent effect on LDHB levels. mRNA levels dropped to 41 ± 20% of control (Fig. 5C).

$^{31}P$ MR spectra (data not shown) indicated that treatment with LY294002 resulted in a decrease in PC to 80 ± 17% relative to control, although this did not reach statistical significance ($P = 0.17$). Similarly, there was a drop to 78% of control in PC following treatment when a cell extract was examined, in line with the decrease of 76 ± 4% ($P = 0.002$, $n = 4$) seen in our previously published study.

**In vivo *studies show a drop in lactate-to-pyruvate ratio.*** To assess the utility of hyperpolarized MRS to monitor PI3K inhibition *in vivo*, we performed a small proof-of-principle study to monitor the effect of everolimus on GS-2 tumor xenografts by probing treatment effect on the lactate-to-pyruvate ratio, as previously described (42). Figure 6 summarizes our findings showing that tumor growth inhibition in treated animals ($n = 2$, dotted lines) was associated with a drop in lactate-to-pyruvate ratio within the tumor. In contrast, tumor growth in control animals ($n = 2$, continuous lines) was associated with an increase in this ratio.

## Discussion

Novel therapeutic approaches are increasingly targeting specific molecular genetic events associated with cancer. These advances are leading to more personalized cancer treatment and are expected to result in improved response and reduced toxicity. However, several challenges remain. Most significantly, many targeted therapies result in tumor stasis rather than shrinkage. Consequently, there is a critical need for noninvasive functional imaging biomarkers that confirm drug delivery and molecular drug activity at the tumor site. Here, we show, to our knowledge for the first time, the application of hyperpolarized $^{13}C$ MRS in the detection of drug target modulation in response to treatment with inhibitors of PI3K signaling.

In this study, PI3K signal inhibition was studied in two cell lines of different cancer types and with different genetic backgrounds. In both cell lines, successful blockade of signaling was associated with a drop in hyperpolarized lactate levels. The drop in hyperpolarized lactate correlated with reduced cellular LDH activity following reduction in HIF-1α levels downstream of PI3K. Further studies are needed to confirm our findings across a wide panel of cell lines. Nonetheless, our initial findings are promising and highlight the potential of hyperpolarized lactate as a biomarker for monitoring the effect of inhibitors of the PI3K pathway.

To assess the potential of this approach for *in vivo* studies, we also performed a limited proof-of-principle study in xenografts. The drop in lactate-to-pyruvate ratio following treatment was in line with the findings in treated cells and likely indicates a drop in the conversion of hyperpolarized pyruvate into lactate within the inhibited tumors. In contrast, the increase in the pyruvate-to-lactate ratio in control tumors is in line with previous work monitoring tumor progression and could be reflecting increased hypoxia and LDH expression within the growing tumor (29). More extensive studies are needed to assess pyruvate metabolism throughout the animal, quantify the dynamics of pyruvate-to-lactate conversion within each voxel, and confirm the underlying biology of the tumor and its mechanistic link to pyruvate metabolism. Nonetheless, this preliminary *in vivo* study shows the feasibility and potential value of hyperpolarized $^{13}C$ studies of pyruvate for noninvasive monitoring of the effect of PI3K inhibitors.

Total lactate levels can also be monitored using $^{1}H$ MRS (44, 45). However, this approach can be of limited utility, particularly *in vivo*. Lactate and lipid peaks usually overlap such that monitoring modulations in lactate can be difficult even when methods for lipid suppression are applied. More importantly, lactate is often associated with poorly vascularized necrotic regions. In this case, the lactate is metabolically inactive and thus would provide little information with regard to the effects of treatment.

The mechanism by which the PI3K pathway interacts with HIF-1 has been thoroughly studied. The PI3K phosphorylation cascade regulates the eIF4F ribosomal complex that is necessary for the translation of HIF-1α (35, 46). In addition, several studies have shown that LY294002 has the ability to reduce HIF-1α levels (47, 48). HIF-1 is responsible for regulating expression of LDHA and other glycolytic enzymes (31, 37). Our results are therefore consistent with these studies, as we show that expression of HIF-1α and LDHA was affected by inhibition of PI3K. This serves to validate our findings by providing the mechanistic underpinnings of hyperpolarized lactate as a biomarker of PI3K signaling.

We have previously shown that PI3K inhibition causes a significant decrease in PC (22). Consistent with these findings, in this study, we also observed a drop in PC in both GS-2 and MDA-MB-231 cells. Importantly, the decrease in PC following PI3K inhibition may be explained by the same mechanism that is controlling the modulation of hyperpolarized lactate (i.e., the drop in HIF-1α levels). The expression of choline kinase, the enzyme responsible for PC synthesis, was recently shown to be regulated by HIF-1 (49). Accordingly, the drop in HIF-1α observed in our treated cells is likely to lead not only to a drop in LDH expression and hyperpolarized lactate formation but also to a drop in choline kinase expression and thus a drop in PC. It should, however, be noted that whereas modulation of PC was observed in this and previous work, it was more modest than the drop in hyperpolarized lactate, required a longer acquisition time, and was more difficult to quantify due to the overlap of PC with other metabolites. This further highlights the value of hyperpolarized lactate as a biomarker of PI3K signal inhibition.

Hyperpolarized $^{13}C$ MRS has now been extensively applied in animal studies and the use of hyperpolarized pyruvate to monitor tumor metabolism is entering clinical trials at our institution. Of note, studies at lower and more clinically relevant field strengths are facilitated by the slightly longer $T_1$ of the carbonyl carbon (50). With this in mind, the work described here shows that hyperpolarized lactate has a promising application as a noninvasive spectroscopic imaging biomarker of PI3K signaling, with potential to inform on drug delivery and efficacy for a range of emerging targeted therapies in future clinical trials.

## Disclosure of Potential Conflicts of Interest

S.J. Nelson, J. Kurhanewicz, D.B. Vigneron, and S.M. Ronen: Commercial research grant, GB Healthcare. The other authors declared no potential conflicts of interest.

## Acknowledgments

We thank Rahwa Iman, Mark Albers, David Joun, Lucas Carvajal, and Samara Nebenzahl for valuable discussions and assistance in performing some of the experiments.

## Grant Support

NIH grants R21 CA120010-01A1 and RO1 CA130819, NIH/National Center for Research Resources UCSF-Clinical and Translational Science Institute grant UL1 RR024131-01, UC Discovery grant ITL-BIO04-10148, and UCSF Brain Tumor Specialized Program of Research Excellence grant CA097257, in conjunction with GE Healthcare.

The costs of publication of this article were defrayed in part by the payment of page charges. This article must therefore be hereby marked *advertisement* in accordance with 18 U.S.C. Section 1734 solely to indicate this fact.

Received 6/22/09; revised 11/4/09; accepted 11/25/09; published OnlineFirst 2/9/10.

## References

1. Fry MJ. Phosphoinositide 3-kinase signalling in breast cancer: how big a role might it play? Breast Cancer Res 2001;3:304–12.
2. Brader S, Eccles SA. Phosphoinositide 3-kinase signalling pathways in tumor progression, invasion and angiogenesis. Tumori 2004;90:2–8.
3. Luo J, Manning BD, Cantley LC. Targeting the PI3K-Akt pathway in human cancer: rationale and promise. Cancer Cell 2003;4:257–62.
4. Samuels Y, Wang Z, Bardelli A, et al. High frequency of mutations of the PIK3CA gene in human cancers. Science 2004;304:554.
5. Hennessy BT, Smith DL, Ram PT, Lu Y, Mills GB. Exploiting the PI3K/AKT pathway for cancer drug discovery. Nat Rev Drug Discov 2005;4:988–1004.
6. Ward S, Sotsios Y, Dowden J, Bruce I, Finan P. Therapeutic potential of phosphoinositide 3-kinase inhibitors. Chem Biol 2003;10:207–13.
7. Workman P, Clarke PA, Guillard S, Raynaud FI. Drugging the PI3 kinome. Nat Biotechnol 2006;24:794–6.
8. Billottet C, Grandage VL, Gale RE, et al. A selective inhibitor of the p110δ isoform of PI 3-kinase inhibits AML cell proliferation and survival and increases the cytotoxic effects of VP16. Oncogene 2006;25:6648–59.
9. Garlich JR, De P, Dey N, et al. A vascular targeted pan phosphoinositide 3-kinase inhibitor prodrug, SF1126, with antitumor and antiangiogenic activity. Cancer Res 2008;68:206–15.
10. Endersby R, Baker SJ. PTEN signaling in brain: neuropathology and tumorigenesis. Oncogene 2008;27:5416–30.
11. Chakravarti A, Palanichamy K. Overcoming therapeutic resistance in malignant gliomas: current practices and future directions. Cancer Treat Res 2008;139:173–89.
12. Yap TA, Garrett MD, Walton MI, Raynaud F, de Bono JS, Workman P. Targeting the PI3K-AKT-mTOR pathway: progress, pitfalls, and promises. Curr Opin Pharmacol 2008;8:393–412.
13. Negendank W. Studies of human tumors by MRS: a review. NMR Biomed 1992;5:303–24.
14. Kvistad KA, Bakken IJ, Gribbestad IS, et al. Characterization of neoplastic and normal human breast tissues with *in vivo* (1)H MR spectroscopy. J Magn Reson Imaging 1999;10:159–64.
15. de Certaines JD, Larsen VA, Podo F, Carpinelli G, Briot O, Henriksen O. *In vivo* $^{31}P$ MRS of experimental tumours. NMR Biomed 1993;6:345–65.
16. Evelhoch JL, Gillies RJ, Karczmar GS, et al. Applications of magnetic resonance in model systems: cancer therapeutics. Neoplasia 2000;2:152–65.
17. Leach MO, Verrill M, Glaholm J, et al. Measurements of human breast cancer using magnetic resonance spectroscopy: a review of clinical measurements and a report of localized $^{31}P$ measurements of response to treatment. NMR Biomed 1998;11:314–40.
18. Vigneron D, Bollen A, McDermott M, et al. Three-dimensional magnetic resonance spectroscopic imaging of histologically confirmed brain tumors. Magn Reson Imaging 2001;19:89–101.
19. Ronen SM, Jackson LE, Beloueche M, Leach MO. Magnetic resonance detects changes in phosphocholine associated with Ras activation and inhibition in NIH 3T3 cells. Br J Cancer 2001;84:691–6.
20. Chung YL, Troy H, Banerji U, et al. Magnetic resonance spectroscopic pharmacodynamic markers of the heat shock protein 90 inhibitor 17-allylamino,17-demethoxygeldanamycin (17AAG) in human colon cancer models. J Natl Cancer Inst 2003;95:1624–33.
21. Beloueche-Babari M, Jackson LE, Al-Saffar NM, Workman P, Leach MO, Ronen SM. Magnetic resonance spectroscopy monitoring of mitogen-activated protein kinase signaling inhibition. Cancer Res 2005;65:3356–63.
22. Beloueche-Babari M, Jackson LE, Al-Saffar NM, et al. Identification of magnetic resonance detectable metabolic changes associated with inhibition of phosphoinositide 3-kinase signaling in human breast cancer cells. Mol Cancer Ther 2006;5:187–96.
23. Koul D, Shen R, Kondo Y, et al. Cellular and *in vivo* activity of a novel PI3K inhibitor PX-866 for treatment of human glioblastoma. Neuro-oncol. In press 2010.
24. Ardenkjaer-Larsen JH, Fridlund B, Gram A, et al. Increase in signal-to-noise ratio of >10,000 times in liquid-state NMR. Proc Natl Acad Sci U S A 2003;100:10158–63.
25. Golman K, Zandt RI, Lerche M, Pehrson R, Ardenkjaer-Larsen JH. Metabolic imaging by hyperpolarized $^{13}C$ magnetic resonance imaging for *in vivo* tumor diagnosis. Cancer Res 2006;66:10855–60.
26. Kohler SJ, Yen Y, Wolber J, et al. *In vivo* 13 carbon metabolic imaging at 3T with hyperpolarized $^{13}C$-1-pyruvate. Magn Reson Med 2007;58:65–9.
27. Day SE, Kettunen MI, Gallagher FA, et al. Detecting tumor response to treatment using hyperpolarized $^{13}C$ magnetic resonance imaging and spectroscopy. Nat Med 2007;13:1382–7.
28. Chen AP, Albers MJ, Cunningham CH, et al. Hyperpolarized C-13 spectroscopic imaging of the TRAMP mouse at 3T—initial experience. Magn Reson Med 2007;58:1099–106.
29. Albers MJ, Bok R, Chen AP, et al. Hyperpolarized $^{13}C$ lactate, pyruvate, and alanine: noninvasive biomarkers for prostate cancer detection and grading. Cancer Res 2008;68:8607–15.
30. Gatenby RA, Gillies RJ. Why do cancers have high aerobic glycolysis? Nat Rev Cancer 2004;4:891–9.
31. Kroemer G, Pouyssegur J. Tumor cell metabolism: cancer's Achilles' heel. Cancer Cell 2008;13:472–82.
32. Semenza GL, Roth PH, Fang HM, Wang GL. Transcriptional regulation of genes encoding glycolytic enzymes by hypoxia-inducible factor 1. J Biol Chem 1994;269:23757–63.
33. Treins C, Giorgetti-Peraldi S, Murdaca J, Semenza GL, Van Obberghen E. Insulin stimulates hypoxia-inducible factor 1 through

a phosphatidylinositol 3-kinase/target of rapamycin-dependent signaling pathway. J Biol Chem 2002;277:27975–81.
34. Arsham AM, Plas DR, Thompson CB, Simon MC. Phosphatidylinositol 3-kinase/Akt signaling is neither required for hypoxic stabilization of HIF-1 α nor sufficient for HIF-1-dependent target gene transcription. J Biol Chem 2002;277:15162–70.
35. Gingras AC, Raught B, Sonenberg N. Regulation of translation initiation by FRAP/mTOR. Genes Dev 2001;15:807–26.
36. Firth JD, Ebert BL, Ratcliffe PJ. Hypoxic regulation of lactate dehydrogenase A. Interaction between hypoxia-inducible factor 1 and cAMP response elements. J Biol Chem 1995;270:21021–7.
37. Pouyssegur J, Dayan F, Mazure NM. Hypoxia signalling in cancer and approaches to enforce tumour regression. Nature 2006;441: 437–43.
38. Ronen SM, Rushkin E, Degani H. Lipid metabolism in T47D human breast cancer cells:$^{31}P$ and $^{13}C$-NMR studies of choline and ethanolamine uptake. Biochim Biophys Acta 1991;1095:5–16.
39. Brindle KM. NMR methods for measuring enzyme kinetics *in vivo*. Prog Nucl Magn Reson Spectrosc 1988;20:257–93.
40. Vassault A. Lactate dehydrogenase. Methods Enzymatic Anal 1983;3.
41. Bernofsky C, Swan M. An improved cycling assay for nicotinamide adenine dinucleotide. Anal Biochem 1973;53:452–8.
42. Park I, Larson P, Zeirhut ML, et al. Hyperpolarized $^{13}C$ MR metabolic imaging: application to brain tumors. Neuro-oncol. In press 2010.
43. Naressi A, Couturier C, Castang I, de Beer R, Graveron-Demilly D. Java-based graphical user interface for MRUI, a software package for quantitation of *in vivo*/medical magnetic resonance spectroscopy signals. Comput Biol Med 2001;31:269–86.
44. Nelson SJ. Multivoxel magnetic resonance spectroscopy of brain tumors. Mol Cancer Ther 2003;2:497–507.
45. Bhujwalla ZM, Glickson JD. Detection of tumor response to radiation therapy by *in vivo* proton MR spectroscopy. Int J Radiat Oncol Biol Phys 1996;36:635–9.
46. Laughner E, Taghavi P, Chiles K, Mahon PC, Semenza GL. HER2 (neu) signaling increases the rate of hypoxia-inducible factor 1α (HIF-1α) synthesis: novel mechanism for HIF-1-mediated vascular endothelial growth factor expression. Mol Cell Biol 2001;21: 3995–4004.
47. Jiang BH, Jiang G, Zheng JZ, Lu Z, Hunter T, Vogt PK. Phosphatidylinositol 3-kinase signaling controls levels of hypoxia-inducible factor 1. Cell Growth Differ 2001;12:363–9.
48. Mabjeesh NJ, Willard MT, Frederickson CE, Zhong H, Simons JW. Androgens stimulate hypoxia-inducible factor 1 activation via autocrine loop of tyrosine kinase receptor/phosphatidylinositol 3′-kinase/protein kinase B in prostate cancer cells. Clin Cancer Res 2003;9: 2416–25.
49. Glunde K, Shah T, Winnard PT, Jr., et al. Hypoxia regulates choline kinase expression through hypoxia-inducible factor-1α signaling in a human prostate cancer model. Cancer Res 2008;68:172–80.
50. Chen AP, Tropp J, Hurd RE, et al. *In vivo* hyperpolarized $^{13}C$ MR spectroscopic imaging with $^{1}H$ decoupling. J Magn Reson 2009; 197:100–6.